LA-UR- 11-03525

Approved for public release; distribution is unlimited.

Title:	Planar Richtmyer-Meshkov Instabilities and Transition to Turbulence
Author(s):	A. Gowardhan, F.F.Grinstein, and J.R. Ristorcelli
Intended for:	Proceedings of the AIAA Computational Fluid Mechanics Conference, Honolulu, Hawaii, 27 - 30 June 2011.

Form 836 (7/06)

Planar Richtmyer-Meshkov Instabilities and Transition to Turbulence

Akshay A. Gowardhan [1], Fernando F. Grinstein.[2], and J. Raymond Ristorcelli [3]
Los Alamos National Laboratory, Los Alamos, NM 87545

A numerical study of the evolution of the multimode planar Richtmyer-Meshkov (RM) instability in a light-heavy (Air-SF6, Atwood number A=0.67) configuration involving a Mach number Ma=1.5 shock is carried out. Our results demonstrate that the initial material interface morphology controls the evolution characteristics of RMI, and provide a significant basis to develop metrics for transition to turbulence. Depending on the initial *rms* slope of the interface, RM evolves into linear or nonlinear regimes, with distinctly different flow features and growth rates, turbulence statistics and material mixing rates. We have called this the bipolar behavior of the RM. An important demonstrated practical consequence of our results is that reshock effects on mixing and transition can be emulated at first shock if the initial rms slope is high enough.

I. Introduction

IN many areas of interest such as, inertial confinement fusion, understanding the collapse of the outer cores of supernovas, and supersonic combustion engines, vorticity is introduced at material interfaces by the impulsive loading of shock waves, and turbulence is generated via Richtmyer-Meshkov (RM) instabilities [1]. RM adds the complexity of shock waves and other compressible effects to the basic physics associated with mixing; compressibility further affects the basic nature of material mixing when mass density and material mixing fluctuation effects are not negligible.

Because shocks and turbulence are involved, resolving all relevant physical scales in RM simulations becomes prohibitively expensive. Turbulent material mixing can be usefully characterized by the fluid physics involved: 1) large-scale entrainment, 2) stirring due to velocity gradient fluctuations, and, 3) molecular diffusion. At moderately high Reynolds number (Re) – when convective time-scales are much smaller than those associated with molecular diffusion, we are primarily concerned with the numerical simulation of the first two convectively-driven (interpenetration) mixing processes, which can be captured with sufficiently resolved implicit large eddy simulation (ILES) [2]. ILES addresses the difficult issues posed by under-resolution, by relying on subgrid models provided implicitly by physics capturing numerics.

Here, we further test ILES using a simulation model that uses the Los Alamos National Laboratory (LANL) RAGE code [3,4] to investigate planar RM. Issues of initial material interface characterization and modeling difficulties, effects of initial condition (IC) resolved spectral content [5] on transitional and late-time turbulent mixing driven by planar RM were investigated. Following on the early RAGE studies of the shocked gas-curtain experiments [3], three-dimensional (3D) simulations of the more recent observations [6,7] were carried out [8] with the aim of characterizing the impact of 3D IC specifics on the shocked gas-curtain dynamics and mixing. The cited work suggests that robust effective performances can be achieved with ILES in the RM context despite uncertainty issues of IC characterization and modeling. Here, we continue our investigation of the effects of initial interfacial morphology of the air-SF6 interface in affecting planar RM [9], with special focus on addressing whether reshock effects on mixing and transition to turbulence can be achieved on first shock.

II. Simulation and Analysis Approach

The planar shock-tube configuration investigated involves low (air) and high (SF6) density gases, presumed ICs at the material interface initially separating the gases, and eventual reshock off an end-wall (Fig. 1). The contact discontinuity between air and SF6 is modeled as a jump in density using ideal gases with γ=1.4 and γ=1.076, respectively, with constant pressure across the initial interface at rest. A shocked air region is created upstream satisfying the Rankine-Hugoniot relations for a Mach 1.5 shock. The shock propagates in the (x) direction through the contact discontinuity (from the light to heavy side) and reflects at the end of the simulation box on the right.

[1] Postdoctoral Research Associate.
[2] Technical Staff Member, Scientist, XCP-4; AIAA Associate Fellow.
[3] Technical Staff Member, Scientist, CCS-2.

Periodic BCs conditions are imposed in the transverse (y,z) directions. The air/SF6 interface is shocked at $t = 0$, reshocked by the primary reflected shock at $t \sim 3.5$ ms, and then by the reflected rarefaction at t ~ 5ms. The material mixing layer is further affected at later times by reflected compression and weaker secondary reflected shock waves. The evolution and interaction of the shock and air/SF6 interface (e.g., Fig.5 in [5]) were in good agreement with those of similar previously reported studies.

RAGE solves the multi-material compressible conservation equations for mass density, momenta, total energy, and partial mass densities, using a 2nd-order Godunov scheme, adaptive mesh refinement (AMR), a variety of numerical options for gradient terms – limiters, and interface treatments. As used in the present work (with no interface treatments, and a van Leer limiter), RAGE models a Schmidt number Sc~1 miscible material interface, and high Reynolds-number (Re) convection-driven flow with effective viscosity ν_{eff} determined by the small-scale cutoff [5].

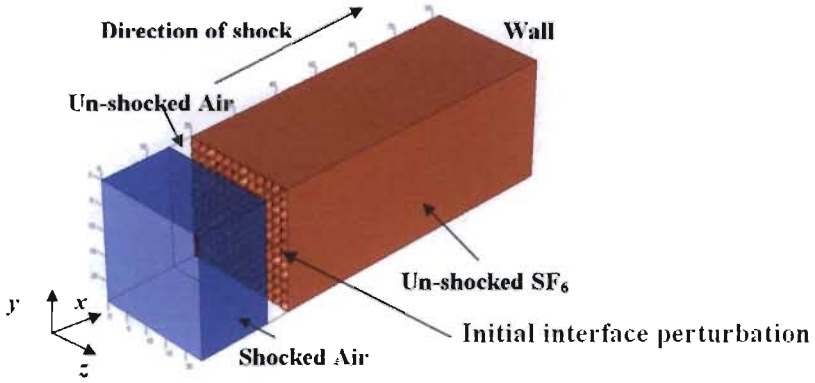

Figure 1. Schematic of the planar shocktube domain.

Integral measure analysis is based on transverse-plane averaged quantities,

$$\langle f \rangle(x) = \frac{1}{A}\int f(x,y,z)dydz \ , \ A = \int dy\,dz,$$

$$Y_{SF_6} = \rho_{SF_6} / \rho, \quad \psi(x) = \langle Y_{SF_6} \rangle, \quad M(x) = 4\psi(x)[1-\psi(x)], \quad \delta(t) = \int M(x)dx,$$

where ρ is the mass density, ρ_{SF6} is the SF_6 partial mass-density, Y_{SF6} is the SF_6 mass fraction, $M(x)$, $\delta(t)$, cross-stream averaged, and integrated mixedness. The instantaneous mixing region is defined by a slab of volume V about the center of the mixing layer constrained in the x-direction by requiring $M(x) > 0.75$. Analysis of turbulence characteristics is based on data deviations around transverse planes within the instantaneous mixing region, using,

$$\tilde{u} = \langle \rho u \rangle / \langle \rho \rangle, \quad u = \tilde{u} + u', \quad \omega = \nabla \times u, \quad 2k = \rho u_i' u_i',$$

$$\rho = \langle \rho \rangle + \rho', \quad R = \rho'^2,$$

$$K = \int k\,dx\,dy\,dz / V, \quad \Omega = \int \rho\omega^2\,dx\,dy\,dz / V,$$

where $\boldsymbol{u}$ is the velocity field, k is the local turbulent kinetic energy, R is the mass-density variance, ω is the vorticity, K and Ω are the mean turbulent kinetic energy and mass-weighted enstrophy, and summation over repeated indices is assumed.

III. Characterizing the Initial Material Interfacial Morphology

The initial interfacial morphology is defined by $\eta_o = \kappa_o \delta_o \sim (\nabla\chi \cdot \nabla\chi)^{1/2}$, the initial *rms* slope, where $\chi(y,z)$ is the local deviation of the initial material interface around the mean interface location, $\kappa_o = 2\pi / \lambda_o$, λ_o is a representative wavelength of the perturbation in the initial interface, and $\delta_o \equiv \delta(t=0)$ denotes the initial interface thickness (Fig.2). Thus, a high value of denotes a highly corrugated interface with high *rms* slope.

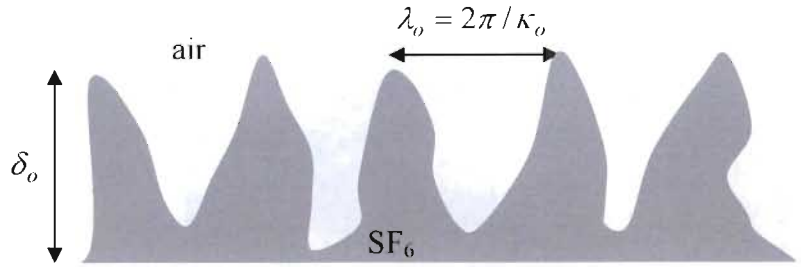

Figure 2. Schematic of the initial material interface characteristics.

The quantity κ_o is used in the study of homogenous stochastic processes, where it is called the mean zero-crossing frequency [10]. In practice, the initial material interface value of is computed by checking for sign changes of the mass density fluctuation over lines within transverse planes and averaging their occurrences (Fig.3); for $t > 0$, $\kappa = \kappa(t)$ is similarly evaluated within the mixing region. Mathematically, κ is associated with $\kappa^2 = \int q^2 E_R(q) dq / \int E_R(q) dq$, where $E_R(q)$ is the instantaneous R spectra in the mixing region, q is the wavenumber, and thus, κ is related to the Taylor microscale; such spectra and connections are exemplified and discussed below.

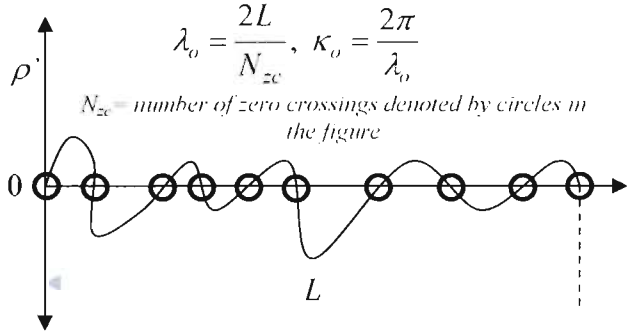

Figure 3. Zero-crossings of ρ'; L denotes the transverse dimension of the computational domain.

Various simulations based experiments were performed in terms of well-defined initial material interface perturbations. The local material interface deformation is given by:

$$\chi(y,z) = \Gamma \sum a_{n,m} \sin(\kappa_n y + \phi_n) \sin(\kappa_m z + \varphi_m),$$

where $\kappa_n = 2\pi n/L$, $\kappa_m = 2\pi m/L$, $-1/2 < a_{n,m} < 1/2$, are random coefficients, Γ is used to prescribe δ_o, $\{\varphi_n, \varphi_m\}$ are random phases, and the participating modes are constrained by the requirement, $\lambda_{min} \le L/[2\pi(n^2 + m^2)^{1/2}] \le \lambda_{max}$. For completeness, we note that for the single-mode classical theoretical analysis [11]. A variety of IC perturbations and grid resolutions (using up to two levels of AMR refinement) were considered. The baseline resolution involved a 820 x 240 x 240 grid (Δ_{min}=0.1cm); a much finely resolved 1640 x 480 x 480 grid (Δ_{min}=0.05cm) was used for selected representative cases. The various cases are organized into two distinct categories having significantly different (low and high) initial *rms* slope (Table 1).

Table 1. Planar Shock-tube Simulations

$(\lambda_{min},\lambda_{max})$	$L(\frac{1}{24},\frac{1}{6})$	$L(\frac{1}{12},\frac{1}{4})$	$L(\frac{1}{6},\frac{1}{3})$	$L(\frac{1}{4},\frac{1}{2})$	$L(\frac{1}{24},\frac{1}{6})$	$L(\frac{1}{12},\frac{1}{4})$	$L(\frac{1}{6},\frac{1}{3})$	$L(\frac{1}{4},\frac{1}{2})$
δ_o (cm)	0.5 (low η_o)				5 (high η_o)			
κ_o (cm^{-1})	π	π /2	π /4	π /6	π	π /2	π /4	π /6

IV. Scaling Integral Mixedness with IC Parameterizations

As noted in our previous related work [5,9], inspection of the evolution of the mixing layer width $\delta(t)$ (Fig.4a) for relatively small η_o (for $\eta_o < \pi/2$), shows growth rates in agreement with predictions of classical linear theory (growth proportional to η_o) [11]. Higher η_o results in larger deposition of baroclinic vorticity which leads to thicker mixing layers. The energy produced by passage of the shock is mostly in the shock direction and leads to growth of the initial modes in that same direction and increased the mixing layer widths. However, for $\eta_o = \pi/2$, the theory is valid only for a very short time after the material interface is shocked. Soon thereafter, the growth rate drops and this is not consistent with linear theory. In contrast, for high η_o ($\eta_o > \pi/2$), the growth is found to be inversely proportional to η_o. For higher η_o there is a much larger deposition of baroclinic vorticity. With the higher η_o interface the vortex centers are closer to each other and they interact, giving rise to the production of more smaller scale modes as is only possible through non-linear processes. Here the energy of the flow, because of the nonlinear interaction, is more isotropically distributed. Interestingly, the increase in η_o does not result in increase in the mixing layer width but leads to production of more small scales and thus more dissipation.

Similarly to the work in [12], we have found useful to plot the layer thickness $\kappa_o(\delta-\delta_o)$ vs. time scaled with $\kappa_o\dot{\delta}_o$ (Fig. 4b), where $\dot{\delta}_o$ is the corresponding initial layer growth rate from the simulations' data. Results for low-η_o and high-η_o collapse into distinctly different correlation groups – suggesting transition to non-linearity above a threshold value $\eta_o \sim \pi/2$. *These results demonstrate what we have denoted the bipolar behavior of RM instabilities* [9].

For interfaces with low-η_o, the growth the mixing layer is *ballistic* with no mode coupling, the evolution of RM is linear ($\sim t$), and follows the scaling of [11]. Increasing η_o in the low-η_o group increases the deposition of baroclinic vorticity on the initial material interface and leads to higher layer growth. In contrast, increasing η_o in the high-η_o group also increases the deposition of baroclinic torque, but this leads to a reduced mixing width growth rate ($\sim t^{0.5}$), associated with the production of small scales by non-linear mode coupling that are additionally dissipative.

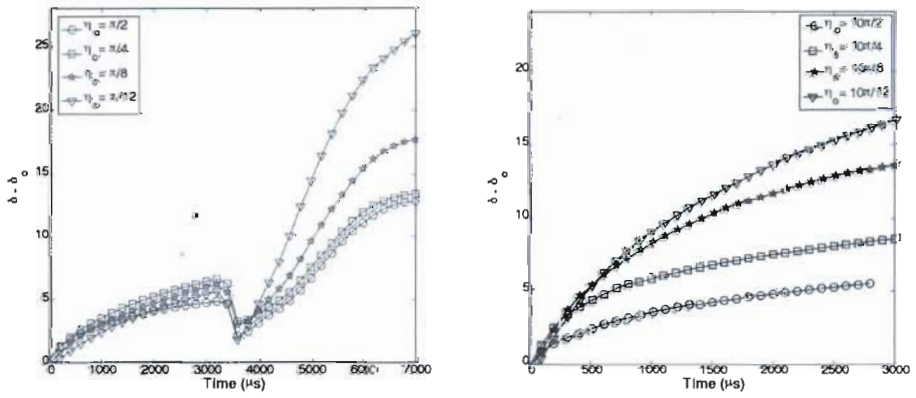

Figure 5. Integral Mixing Width. (a, left): low-η_o (reshocked); (b, right): high-η_o (shocked)

V. Can Transition to Turbulence Occur on First-Shock ?

Our analysis above on the effects of initial interfacial morphology indicate that for high η_o, RM develops into a non linear regime and transition to turbulence is suggested. In what follows, we systematically compare reshocked low-η_o results with first-shock high-η_o results. The reshock wall is located such that reshock impacts the material interface at ~ 4000 μs.

Figure 5(a) shows the growth of mixing layer for the low-η_o cases. It can be observed that before reshock, the growth of mixing layer is consistent with Richtmyer's classical theory, i.e. growth is proportional to η_o of the

interface. However, after reshock, the growth trends reverses and is now consistent with the non linear regime (Fig. 5(b)). This shows that integral mixedness growth trends for shocked high-η_o are consistent with those of reshocked low-η_o.

Figure 6a shows the evolution of the simulated Taylor microscale $\kappa(t)$ for the low-η_o case. Before reshock, $\kappa(t)$ is virtually constant. When the mixing layer is reshocked, $\kappa(t)$ jumps suddenly indicating smaller-scale production. Similar effects are seen for high-η_o case at first shock (Fig. 6b).

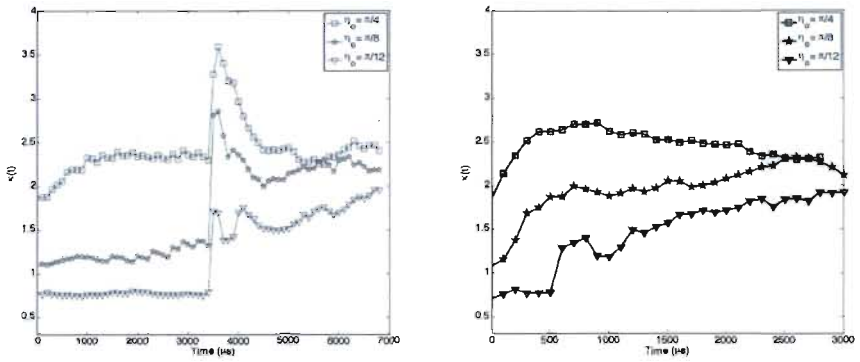

Figure 6. Taylor Microscale. (a, left): low-η_o (reshocked); (b, right): high-η_o (shocked)

Figures 7 and 8 show the computed evolution of the mean turbulent kinetic energy K and mean mass-weighted enstrophy Ω for low-η_o and high-η_o cases. After reshock, non-linear mode coupling increases the population of small scales (higher $\kappa(t)$ in Fig. 4), increasing Ω (Fig. 8), which dissipates K *faster* (i.e., following $-dK/d\,t \sim 2v_{eff}\Omega$) – thus reducing K (Fig.7). For the low-η_o group there is no mode coupling and no production of new small scales before reshock, and the evolution of K follows closely that of Ω. Figure 7a shows the evolution of K with time for the low-η_o case. Before reshock, K increases with increasing η_o; after reshock, K decreases with increase in η_o – similarly to the shocked high-η_o case.

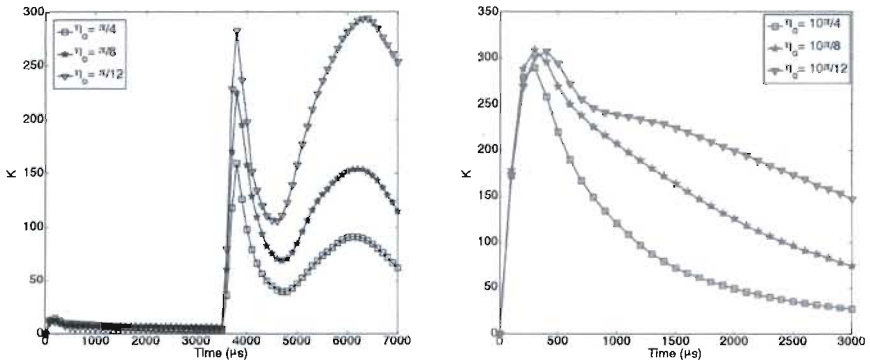

Figure 7. Mean Turbulent Kinetic Energy. (a, left): low-η_o (reshocked); (b, right): high-η_o (shocked)

Transition to turbulence is suggested by a rapid increase in population of motions with smaller length scales, which can lead to an inertial subrange in the turbulent kinetic energy spectra [13]. The spectral bandwidth turbulence can be scaled by the turbulent Reynolds number [14], usually taken as a ratio of integral-to-Kolmogorov length scales. In our context, we use the thickness of the layer, $\delta(t)$ as a measure of the integral scale, and the mass-density Taylor micro-scale $\lambda(t)$ – related to the spatial zero crossing frequency through $\lambda(t) \sim 1/\kappa(t)$ – as proxy for the small scales. We use $\eta(t) = \kappa(t)\delta(t)$ as measure of the *spectral bandwidth*. Figure 9 indicates that the *rms* slope of the interface $\eta(t)$ increases with time. Just before reshock time (~4000 μs), $\eta(t)$ ives the initial *rms* slope for the reshock problem, and when $\eta(t) > \pi$, it is high enough for transition to turbulence to become possible.

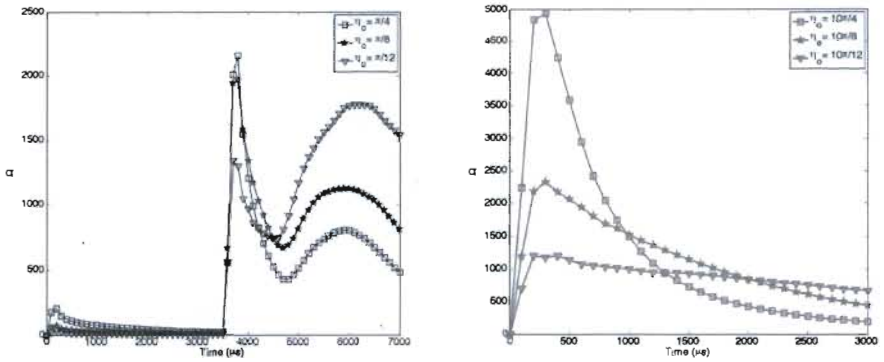

Figure 8. Mean Enstrophy. (a, left): low-η_o (reshocked); (b, right): high-η_o (shocked)

Figure 10 shows the evolution of $\eta(t)$ after the mixing layer is shocked. The fact that $\eta(t)$ increases with time for all cases suggests that spectral bandwidth is increasing (which can also be understood as an increase in turbulent Reynolds number). The late time saturation of $\eta(t)$ for the highest η_o in Fig. 10, indicates faster disappearance by dissipation of the smallest scales of the flow. Due to mode coupling there is a much larger (and faster) increase in spectral bandwidth for the high-η_o group. Our observations suggest that sudden increase in $\eta(t)$ (and $\kappa(t)$) can be consistently used as metrics to indicate flow transition.

Mixing visualizations in shocked high-η_o and shocked / reshocked low-η_o cases are shown in Fig. 11 in terms of volume distributions of mass fraction of SF_6 at selected times, t=3000 μs after the first shock (or t=3000 μs after reshock). Figure 11 indicates that they exhibit qualitative similar mixing features; shocked low-η_o shows distinctly less mixing as compared to the other two cases. Figure 12 shows the PDF of mass fraction of SF_6 at the same selected times. PDFs (Fig. 12b) for the shocked high-η_o and reshocked low-η_o show similar features, however the PDF (Fig. 12a) for shocked low-η_o shows high value for pure fluids indicating less mixing.

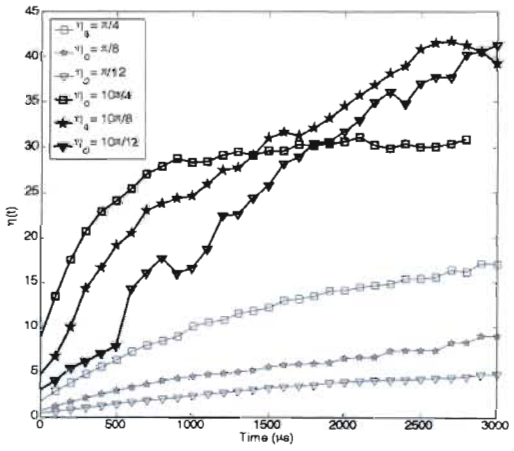

Figure 9. Spectral Bandwidth.

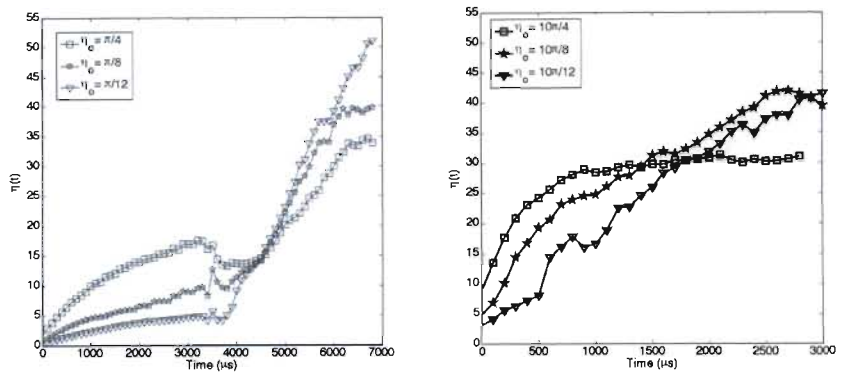

Figure 10. Spectral Bandwidth. (a, left): low-η_o (reshocked); (b, right): high-η_o (shocked)

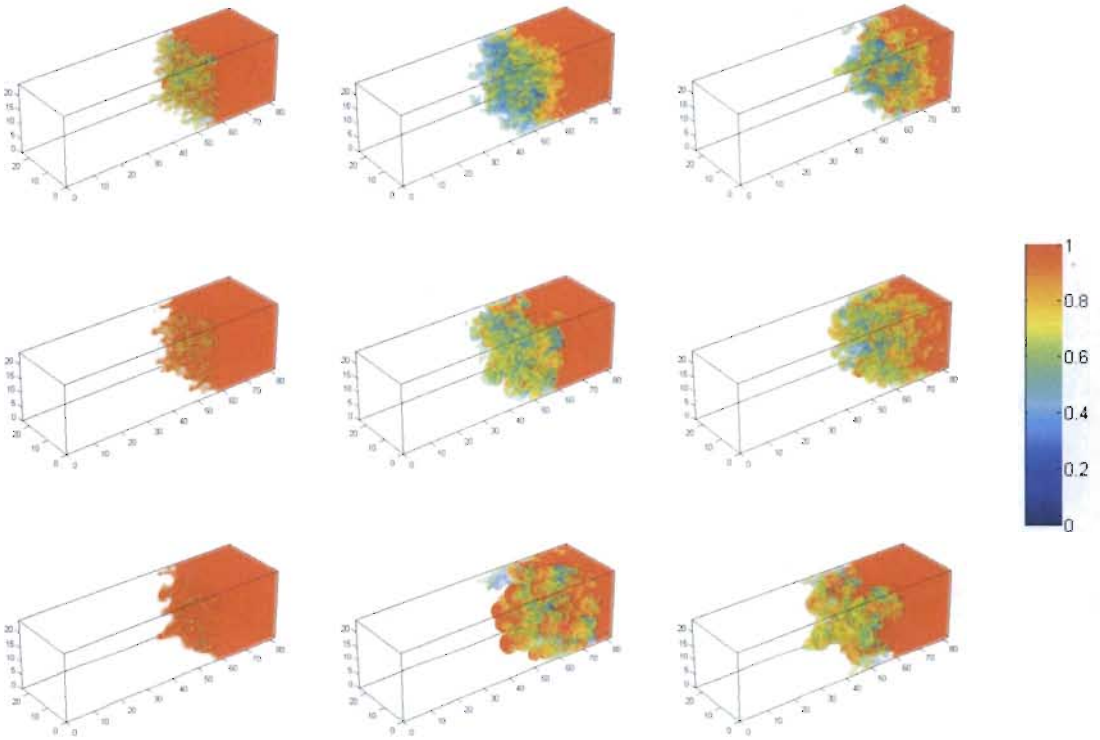

Figure 11. Mixing Visualizations. left: low-η_o (shocked); center: low-η_o (reshocked); right: high-η_o (shocked); selected representative times: t=3000 μs after the first shock (or t=3000 μs after reshock)

VI. Conclusion

We examined the effects of initial interfacial morphology of the *air-SF_6* interface in affecting planar RM. Vorticity production at shock time and eventual mode coupling (and transition) thereafter will depend on the initial interfacial characteristics, as well as on the particular A, Ma, and (light/heavy or heavy/light) configuration considered. However, the initial *rms* slope of the material interface appears to be a relevant parameter in determining whether the flow is in the linear ballistic regime, or in non-linear mode coupling and transition to turbulence regime. We have called this the *bipolar behavior of the RM instability;* we have been able to recognize this behavior also in our shocked gas-curtain shocktube studies [15].

In the linear regime, the impulsive theory [11] predicts the mixing layer growth trends: as the initial *rms* slope increases the growth rate increases. Less mode coupling is seen, as inferred by the smaller spectral bandwidth, and the primary production of enstrophy is baroclinic. In the nonlinear regime, the mixing layer growth rate trends are the inverse of that predicted by the theory. There is significant mode coupling and our proxy for spectral bandwidth makes a sudden jump which we associate with a transition to turbulence; this suggests that stretching becomes an important enstrophy production mechanism.

Some of our findings for the nonlinear regime are not consistent with heuristic notions one might have of statistically steady turbulence, and are likely a consequence of the non-equilibrium nature of the RMI. The fact that slower growth rate of the mixing-layer width is associated with more material (interpenetration) mixing demonstrates that mixing-layer width growth-rate, bulk *Re*, and material mixing are not causally connected. Our observations have a very straightforward physical explanation: higher initial material interface slopes lead to production of more smaller scales which dissipate turbulent kinetic energy faster, reducing the growth rate. An important practical consequence of our results is that reshock effects on mixing and transition can be emulated at first shock if η_o is high enough.

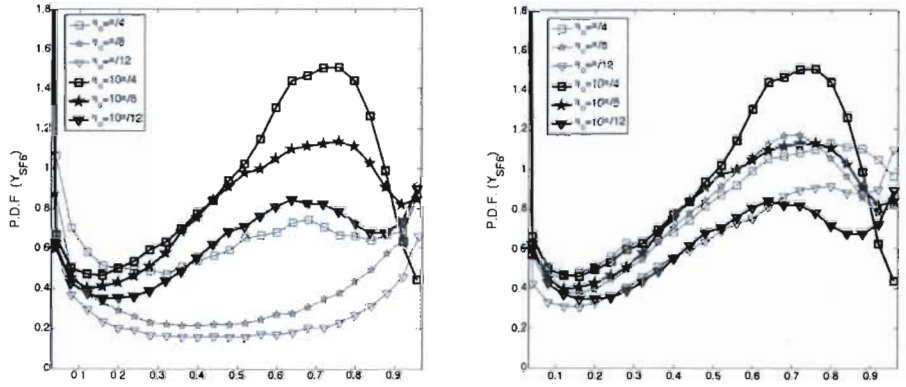

Figure 12. PDFs of Y_{SF6}; left: shocked high-η_o *vs.* shocked low-η_o ; right: shocked high-η_o *vs.* reshocked low-η_o); selected times as in Fig.12.

Acknowledgments

LANL is operated by the Los Alamos National Security, LLC for the U.S. Department of Energy NNSA under Contract No. DE-AC52-06NA25396. This work was made possible by funding from the Laboratory Directed Research and Development Program on "Turbulence by Design" at LANL through directed research project number 20090058DR.

References

1. Brouillete, M., "The Ritchmyer-Meshkov instability", Annu. Rev. Fluid Mech., 34, 445-468, 2002.
2. F.F. Grinstein, L.G. Margolin, and W.J. Rider 2007, Eds., Implicit Large Eddy Simulation: Computing Turbulent Flow Dynamics, Cambridge University Press, New York.
3. Baltrusaitis, R. M., Gittings, M. L., Weaver, R. P., Benjamin, R. F. & Budzinski, J. M. 1996, Simulation of shock-generated instabilities, Phys. Fluids 8, 2471-2483.
4. Gittings, M., Weaver, R. , Clover, M. , Betlach, T. , Byrne, N. , Coker, R. , Dendy, E., Hueckstaedt, R. , New, K. , Oakes, W. R. , Ranta, D. , Stefan, R. , "The RAGE Radiation-Hydrodynamic Code", Comput. Science & Discovery 1 (2008) 015005.
5. F.F. Grinstein, A.A. Gowardhan, and A.J. Wachtor, "Simulations of Richtmyer-Meshkov Instabilities in Planar Shock-Tube Experiments", Phys. Fluids, 23, 034106 (2011).
6. Balakumar, B.J., Orlicz, G., Tomkins, C. and Prestridge, K., "Simultaneous particle-image velocimetry–planar laser-induced fluorescence measurements of Richtmyer–Meshkov instability growth in a gas curtain with and without reshock", Phys. Fluids, 20, 124103, 2008.
7. G. C. Orlicz, B. J. Balakumar, C. D. Tomkins, and K. P. Prestridge, "A Mach number study of the Richtmyer–Meshkov instability in a varicose, heavy-gas curtain", Phys. Fluids, 21, 064102, 2009.
8. A.A. Gowardhan and F.F. Grinstein, "Numerical Simulation of Richtmyer-Meshkov Instabilities in Shocked Gas-Curtains", submitted to Journal of Turbulence (2011).

9. A.A. Gowardhan, J. R. Ristorcelli, and F.F. Grinstein, "The Bipolar Behavior of the Richtmyer-Meshkov Instability", submitted to Phys. Fluids (2011).
10. K R Sreenivasan, A Prabhu & R Narasimha, "Zero-crossings in turbulent signals", J. Fluid Mechanics, 137, 251-272 (1983).
11. Richtmyer, R. D., 1960: "Taylor instability in shock acceleration of compressible fluids". Commun. Pure Appl. Maths. 13, 297–319.
12. Jacobs, J.W. and Sheeley, J.M., "Experimental Study of Incompressible Richtmyer- Meshkov Instability". Physics of Fluids. 8, 405-15 (1996).
13. Y. Zhou, "Unification and extension of the similarity scaling criteria and mixing transition for studying astrophysics using high energy density laboratory experiments or numerical simulations", Physics of Plasmas, 14, 082701 (2007).
14. Tennekes, H. and J. L. Lumley, A First Course in Turbulence, MIT Press, Cambridge, MA, 1972.
15. A.A. Gowardhan, S. Balasubramanian, F.F. Grinstein, K.P. Prestridge, and J.R. Ristorcelli, "Analysis of Computational and Laboratory Shocked Gas-Curtain Experiments", 2011 AIAA Summer Fluids Conferences, Honolulu, Hawaii, AIAA, Reston, VA (submitted for publication).